Constructing the finite-volume equations for cosmological MGFLD

Daniel R. Reynolds

October 7, 2014

1 Base cosmological FLD equation

The radiation energy density, flux, and pressure tensor are related to the specific intensity moments via the relations

$$E_\nu = \frac{4\pi}{c} J_\nu = \frac{1}{c} \oint I_\nu \, d\Omega, \tag{1}$$

$$\mathbf{F}_\nu^i = 4\pi H_\nu^i = \oint \vec{n}^i I_\nu \, d\Omega, \tag{2}$$

$$\overline{\mathbf{P}}_\nu^{ij} = \frac{4\pi}{c} K_\nu^{ij} = \frac{1}{c} \oint \vec{n}^i \vec{n}^j I_\nu \, d\Omega, \tag{3}$$

where each of these are defined in proper, CGS units. For frequencies $\nu \in \mathbb{R}^+$, times $t \in \mathbb{R}$ and spatial locations $\mathbf{r} \in \mathbb{R}^3$, we denote the domain of these functions as $\bar{\Omega} = \mathbb{R}^+ \times \mathbb{R} \times \mathbb{R}^3$. Then $I_\nu : \bar{\Omega} \to \mathbb{R}$ is the specific radiation intensity, $E_\nu : \bar{\Omega} \to \mathbb{R}$ is the radiation energy density (erg cm^{-3} Hz^{-1}), $\mathbf{F}_\nu : \bar{\Omega} \to \mathbb{R}^3$ is the radiation energy flux, and $\overline{\mathbf{P}}_\nu : \bar{\Omega} \to \mathbb{R}^{3\times 3}$ is the radiation pressure tensor.

The moment equations for a generalized fluid coupled with a radiation fluid for a cosmological medium are as follows (c.f. [1, 3]). The zeroth moment of the Boltzmann equation provides an evolution equation for the radiation energy density,

$$\partial_t E_\nu + \nabla \cdot (E_\nu \mathbf{v}_b) + \nabla \cdot \mathbf{F}_\nu + \overline{\mathbf{P}}_\nu : (\nabla \mathbf{v}_b) + \frac{3\dot{a}}{a} E_\nu - \frac{\nu \dot{a}}{a} \partial_\nu E_\nu = \eta_\nu - c\kappa_\nu E_\nu. \tag{4}$$

Here, $\eta_\nu : \bar{\Omega} \to \mathbb{R}$ is the emissivity source (g cm^{-1} s^{-2}). $\kappa_\nu : \bar{\Omega} \to \mathbb{R}$ is the combined opacity (cm^{-1}) due to the elemental species, and is computed as

$$\kappa_\nu = \sum_{i=1}^{N_{\text{chem}}} \sigma_i(\nu) \, \mathtt{n}_i, \tag{5}$$

where $\sigma_i(\nu)$ is the cross-section of the elemental species $\mathtt{n}_i$. We note that in the above equation (and the remainder of this document), the spatial derivatives denoted by ∇ are taken with respect to the proper position, $\mathbf{r}$.

Similarly, the first moment of the Boltzmann equation provides an evolution equation for the radiation energy flux,

$$\partial_t \mathbf{F}_\nu + \nabla \left(\mathbf{F}_\nu \cdot \mathbf{v}_b \right) + c^2 \nabla \cdot \overline{\mathbf{P}}_\nu + \left(\mathbf{F}_\nu \cdot \nabla \right) \mathbf{v}_b + \frac{3\dot{a}}{a} \mathbf{F}_\nu - \frac{\nu \dot{a}}{a} \partial_\nu \mathbf{F}_\nu = -c\kappa_\nu \mathbf{F}_\nu. \tag{6}$$

1.1 Flux Limited Diffusion approximation

For a flux limited diffusion (FLD) approximation, the radiative flux vector is computed as a function of the energy density gradient through a parameterization,

$$\mathbf{F}_\nu = -D\,\nabla E_\nu, \tag{7}$$

where $D : \bar{\Omega} \to \mathbb{R}^{3\times 3}$ is the *flux limiter* ($\mathrm{cm}^2\ \mathrm{s}^{-1}$) that depends on both the opacity κ_ν, and the radiation energy density E_ν.

Using the FLD approximation, the equation (6) may be ignored, and the zeroth moment equation (4) becomes

$$\partial_t E_\nu + \nabla\cdot(E_\nu \mathbf{v}_b) - \nabla\cdot(D\,\nabla E_\nu) - \frac{1}{c}\left(\nabla(D\,\nabla E_\nu)\right) : (\nabla \mathbf{v}_b) + \frac{3\dot{a}}{a}E_\nu - \frac{\nu\dot{a}}{a}\partial_\nu E_\nu = \eta_\nu - c\kappa_\nu E_\nu, \tag{8}$$

where we have used the FLD-based approximation of the radiation pressure as $\overline{\mathbf{P}}_\nu = \frac{1}{c}\nabla\mathbf{F}_\nu = -\frac{1}{c}\nabla\left(D\,\nabla E_\nu\right)$. Note that in general, $\overline{\mathbf{P}}_\nu$ is non-symmetric, due to the spatial dependence of the flux-limiter D. The equation (8) is an equation defining the scalar-valued variable E_ν, that may either be solved independently, or coupled with the elemental densities $\mathtt{n}_i$ and hydrodynamic quantities of the the fluid energy e, velocity $\mathbf{v}_b$ and density ρ_b.

For conditions that allow omission of the radiation pressure term, the zeroth moment equations corresponding to (4) can be simplified to

$$\partial_t E_\nu + \nabla\cdot(E_\nu \mathbf{v}_b) - \nabla\cdot(D\,\nabla E_\nu) + \frac{3\dot{a}}{a}E_\nu - \frac{\nu\dot{a}}{a}\partial_\nu E_\nu = \eta_\nu - c\kappa_\nu E_\nu. \tag{9}$$

The equation (9) is a reaction-advection-diffusion equation, that is again a function of the energy density E_ν, though here is parabolic in nature, in that it describes a diffusion-like radiation transport.

Lastly, since Enzo performs a second-order-accurate piecewise parabolic algorithm for hydrodynamic advection, with passive advection of other density-like quantities (including E_ν), in considering a new solver for evolving only the radiation field, we may consider the simpler reaction-diffusion equation

$$\partial_t E_\nu - \nabla\cdot(D_\nu\,\nabla E_\nu) + \frac{3\dot{a}}{a}E_\nu - \frac{\nu\dot{a}}{a}\partial_\nu E_\nu = \eta_\nu - c\kappa_\nu E_\nu. \tag{10}$$

As previously mentioned, the role of the flux limiter D is one of providing a continuous transition between the isotropic and free-streaming limits. To this end, we consider the flux limiter to operate independently in each Cartesian direction,

$$D_\nu(\kappa_\nu, E_\nu) = \begin{bmatrix} D_{\nu,1}(\kappa_\nu, E_\nu) & 0 & 0 \\ 0 & D_{\nu,2}(\kappa_\nu, E_\nu) & 0 \\ 0 & 0 & D_{\nu,3}(\kappa_\nu, E_\nu) \end{bmatrix},$$

where we employ a limiter of the form [2]:

$$D_{\nu,i} = c\left(9\kappa_\nu^2 + R_{\nu,i}^2\right)^{-1/2}, \quad i = 1,2,3, \tag{11}$$

$$R_{\nu,i} = \frac{|\partial_{\mathbf{r}_i} E_\nu|}{E_\nu}, \quad i = 1,2,3. \tag{12}$$

We elaborate further on the implementation of these formulas in Section 4.

1.2 Multi-Frequency Approximation

Our first approximation to the radiation energy density equation (10) will be to remove the dependency on frequency space by choosing to evolve radiation energy densities at a specific set of frequencies. To this end,

let us denote a finite set of frequencies as

$$\nu_1 < \nu_2 < \cdots < \nu_{N_f}. \tag{13}$$

We may then consider the full frequency-dependent radiation field to be comprised of radiation emitted only at this finite set of frequencies. Under this "multi-frequency" discretization, we may consider the overall frequency-dependent radiation energy density function to have the form

$$E_\nu(t, \mathbf{r}, \nu) = \sum_{\omega=1}^{N_f} E_\omega(t, \mathbf{r})\, \delta_{\nu_\omega}(\nu), \tag{14}$$

where $\delta_{\nu_\omega}(\nu)$ is the Dirac delta function (with units of Hz^{-1}), and where we have defined a set of monochromatic radiation energy densities, $E_1, E_2, \ldots, E_{N_f}$. We note that with this definition, each radiation energy field, E_ω has units of energy density (ergs cm^{-3}), unlike the original frequency-dependent radiation energy E_ν that had units ergs cm^{-3} Hz^{-1}. Under this approximation, the equation (10) is only defined at each of the frequencies ν_ω, $\omega = 1, \ldots, N_f$. By integrating the equation (10) over frequency space, we obtain a set of N_f independent equations, one at each specific frequency ν_ω,

$$\partial_t E_\omega - \nabla \cdot (D_\omega \nabla E_\omega) + \frac{4\dot{a}}{a} E_\omega = \eta_\omega - c\kappa_\omega E_\omega, \qquad \omega = 1, \ldots, N_f. \tag{15}$$

We note that since each of these frequencies solves the equation at a different ν_ω, the frequency-space coupling term $\frac{\nu\dot{a}}{a}\partial_\nu E_\nu$ from equation (10) has been omitted. We further note that each of these monochromatic radiation energy densities is only a function of space and time, i.e. $E_\omega = E_\omega(t, \mathbf{r})$.

In the above transformation of the equation (10) to the system of equations (15), we elaborate on three non-trivial terms, the opacity κ_ω, emissivity η_ω and the cosmological expansion term $4\frac{\dot{a}}{a}E_\omega$. The first of these may simply be defined through evaluating the corresponding multi-frequency opacity at the associated frequency ν_ω, i.e.

$$\kappa_\omega(t, \mathbf{r}) = \kappa_\nu(t, \mathbf{r}, \nu_\omega) = \sum_{i=1}^{N_{\mathrm{chem}}} \mathtt{n}_i(t, \mathbf{r})\, \sigma_{\mathtt{n}_i}(\nu_\omega). \tag{16}$$

The resulting frequency-specific opacity κ_ω therefore retains the units of cm^{-1}.

We define emissivity for each of these radiation fields through taking the corresponding multi-frequency emissivity and integrating over frequency space, as was performed to the equations themselves. We note that in order for this integrated emissivity to be usable within the discrete single-frequency equations (15), we must assum that the multi-frequency emissivity admits a form similar to (14), i.e. we assume that

$$\eta_\nu(t, \mathbf{r}, \nu) = \sum_{\omega=1}^{N_f} \eta_\omega(t, \mathbf{r})\, \delta_{\nu_\omega}(\nu), \tag{17}$$

The resulting frequency-specific emissivity η_ω therefore has units of ergs cm^{-3} s^{-1}, corresponding to the rate of energy density emission at the frequency ν_ω.

The term that corresponds to cosmological expansion, $4\frac{\dot{a}}{a}E_\omega$, results from the two terms in the original equation, $\frac{3\dot{a}}{a}E_\nu - \frac{\nu\dot{a}}{a}\partial_\nu E_\nu$. Specifically, the second of these reduces to $\frac{\dot{a}}{a}E_\omega$ through integration by parts,

$$\begin{aligned}
\frac{\nu\dot{a}}{a}\partial_\nu E_\nu \;\rightarrow\; \int_0^\infty \frac{\nu\dot{a}}{a}\partial_\nu E_\nu \,\mathrm{d}\nu &= \frac{\dot{a}}{a}\sum_{\omega=1}^{N_f} E_\omega \int_0^\infty \nu\, \partial_\nu \delta_{\nu_\omega}(\nu)\,\mathrm{d}\nu \\
&= \frac{\dot{a}}{a}\sum_{\omega=1}^{N_f} E_\omega \left[(\nu\, \delta_{\nu_\omega})\Big|_0^\infty - \int_0^\infty \delta_{\nu_\omega}\,\mathrm{d}\nu\right] \\
&= \frac{\dot{a}}{a}\sum_{\omega=1}^{N_f} E_\omega\,[0-1] = -\frac{\dot{a}}{a}\sum_{\omega=1}^{N_f} E_\omega.
\end{aligned} \tag{18}$$

As with the other terms in equation (15), each portion of this sum is evolved separately, along with the other terms at each frequency ν_ω.

Additionally, we may define the photo-heating and photo-ionization terms that couple these radiation fields to the matter. First, we compute the frequency-integrated photoionization rate Γ_i^{ph} for each chemical species $\mathtt{n}_i$ as

$$\Gamma_i^{ph}(t,\mathbf{r}) = c\int_{\bar{\nu}_i}^{\infty} \frac{\sigma_{\mathtt{n}_i}(\nu)E_\nu(t,\mathbf{r},\nu)}{h\nu}\,\mathrm{d}\nu = \sum_{\omega=1}^{N_f} \frac{c\,E_\omega(t,\mathbf{r})}{h}\left(\frac{\sigma_{\mathtt{n}_i}(\nu_\omega)}{\nu_\omega}\right), \qquad i = 1,\ldots,N_{\text{chem}}, \tag{19}$$

where here we denote the ionization threshold frequency for species $\mathtt{n}_i$ as $\bar{\nu}_i$. Furthermore, in this equation we have implicitly assumed that the species cross-sections satisfy $\sigma_{\mathtt{n}_i}(\nu) = 0$ for all $\nu < \bar{\nu}_i$, which is sufficient to guarantee that monochromatic radiation energy densities at frequencies below $\bar{\nu}_i$ do not contribute to the photoionization rate $\Gamma_i^{ph}(t,\mathbf{r})$.

Similarly, we compute the frequency-integrated specific photoheating rate, G, using our multi-frequency radiation field (14) as

$$\begin{aligned} G(t,\mathbf{r}) &= \sum_{i=1}^{N_{\text{chem}}} \frac{c\,\mathtt{n}_i}{\rho_b}\int_{\bar{\nu}_i}^{\infty} \sigma_{\mathtt{n}_i}(\nu)E_\nu(t,\mathbf{r},\nu)\left(\frac{h\nu - h\bar{\nu}_i}{h\nu}\right)\mathrm{d}\nu \\ &= \sum_{i=1}^{N_{\text{chem}}} \frac{c\,\mathtt{n}_i}{\rho_b}\int_{\bar{\nu}_i}^{\infty} \sigma_{\mathtt{n}_i}(\nu)E_\nu(t,\mathbf{r},\nu)\left(1 - \frac{\bar{\nu}_i}{\nu}\right)\mathrm{d}\nu \\ &= \sum_{i=1}^{N_{\text{chem}}}\sum_{\omega=1}^{N_f} \frac{c\,\mathtt{n}_i\,E_\omega(t,\mathbf{r})}{\rho_b}\left[\sigma_{\mathtt{n}_i}(\nu_\omega)\left(1 - \frac{\bar{\nu}_i}{\nu_\omega}\right)\right]. \end{aligned} \tag{20}$$

1.3 Multi-Group Approximation

As an alternative discretization of the frequency-dependent radiation energy density equation (10), we may choose to evolve groups of radiation energy densities defined within frequency bands, or bins. We again consider the derivation of N_f radiation fields, each of which is now defined over a frequency band. To this end, we define the set of frequency bands

$$\nu_{\omega,L} < \nu_{\omega,R}, \quad \omega = 1,\ldots,N_f. \tag{21}$$

These values define frequency *groups*,

$$g_1 = [\nu_{1,L},\nu_{1,R}), \qquad g_2 = [\nu_{2,L},\nu_{2,R}), \qquad \cdots \qquad g_{N_f} = [\nu_{N_f,L},\nu_{N_f,R}). \tag{22}$$

We may then consider the full frequency-dependent radiation field to be comprised of radiation emitted uniformly *within* each group, but non-uniformly *between* groups. Under this "multi-group" discretization, we may consider the overall frequency-dependent radiation energy density function to have the piecewise constant form

$$E_\nu(t,\mathbf{r},\nu) = \begin{cases} \frac{1}{|g_\omega|}E_\omega(t,\mathbf{r}), & \text{if} \quad \nu \in g_\omega,\ \omega = 1,\ldots,N_f \\ 0, & \text{otherwise,} \end{cases} \tag{23}$$

where $|g_\omega| = \nu_{\omega,R} - \nu_{\omega,L}$ is the width of the frequency group.

Notes:

(i) Each radiation energy group, E_ω has units of energy density (ergs cm^{-3}), unlike the original frequency-dependent radiation energy E_ν that had units ergs cm^{-3} Hz^{-1}.

(ii) Under this discretization, the "standard" multi-group definition has contiguous frequency bands, i.e. neighboring bands satisfy $\nu_{\omega,R} = \nu_{\omega+1,L}$.

(iii) Under this discretization, the radiation field is no longer continuous as a function of frequency. For example, in Figure 1 we show a continuous $T = 10^5$ blackbody radiation spectrum (left), along with its contiguous 5 and 10 group approximations (center and right). We note that these plots show the values of $\frac{1}{|g_\omega|}E_\omega$, that approximate the values of E_ν.

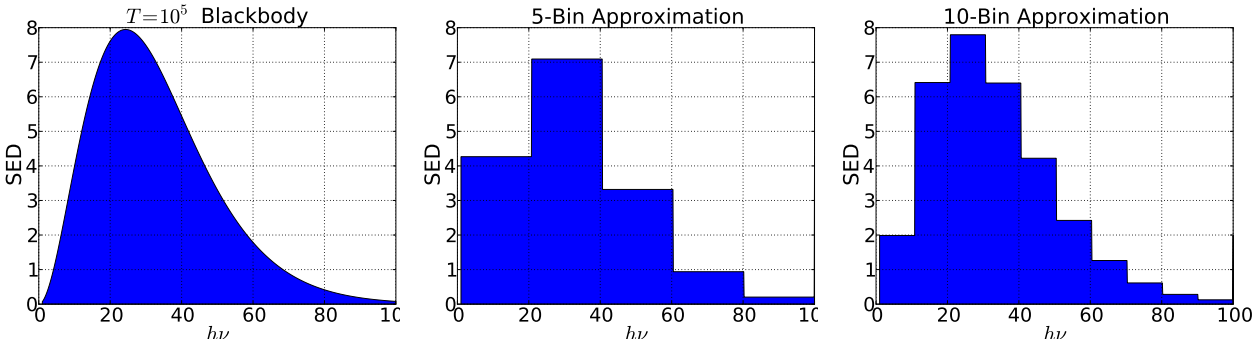

Figure 1: Comparison between true $T = 10^5$ blackbody radiation spectral energy distribution and its contiguous 5 and 10 group counterparts.

(iv) This piecewise constant approximation of the underlying frequency dependence of E_ν is only first-order accurate as a function of the bin width.

(v) Under this discretization, we also allow for gaps in the radiation spectrum (i.e. non-contiguous frequency bands). For example, if one wanted a crude approximation to separately transporting both UV and X-ray radiation, a two-bin approach with $g_1 = [13.6, 100)$ and $g_2 = [500, 10000)$ could be used.

(vi) To ensure photon conservation, these bins must be filled with the total amount of E_ν within each bin, *not* the value at the central frequency, i.e.

$$E_\omega(t, \mathbf{r}) = \int_{\nu_{\omega,L}}^{\nu_{\omega,R}} E_\nu(t, \mathbf{r}, \nu)\,\mathrm{d}\nu, \quad \omega = 1, \ldots, N_f.$$

This applies to both initial conditions, and (more importantly) to the emissivity values that source each radiation group.

With this approximation in place, we may consider the implications on solving the radiation energy density equation (10). Due to the piecewise constant radiation approximation, we simplify the equation (10) by integrating over each frequency group. As a result, instead of solving a single frequency-dependent equation (10), we now have separate equations for each radiation group. We investigate each term separately,

$$\partial_t E_\nu \;\rightarrow\; \int_{\nu_{\omega,L}}^{\nu_{\omega,R}} \partial_t E_\nu\,\mathrm{d}\nu = \partial_t \left(\int_{\nu_{\omega,L}}^{\nu_{\omega,R}} E_\nu\,\mathrm{d}\nu \right) = \partial_t E_\omega, \tag{24}$$

$$\nabla \cdot (D_\nu \nabla E_\nu) \;\rightarrow\; \int_{\nu_{\omega,L}}^{\nu_{\omega,R}} \nabla \cdot (D_\nu \nabla E_\nu)\,\mathrm{d}\nu = \nabla \cdot (D_\omega \nabla E_\omega), \tag{25}$$

$$\frac{3\dot{a}}{a} E_\nu \;\rightarrow\; \int_{\nu_{\omega,L}}^{\nu_{\omega,R}} \frac{3\dot{a}}{a} E_\nu\,\mathrm{d}\nu = \frac{3\dot{a}}{a} E_\omega, \tag{26}$$

$$\eta_\nu \;\rightarrow\; \int_{\nu_{\omega,L}}^{\nu_{\omega,R}} \eta_\nu\,\mathrm{d}\nu \equiv \eta_\omega, \tag{27}$$

$$c\kappa_\nu E_\nu \;\rightarrow\; \int_{\nu_{\omega,L}}^{\nu_{\omega,R}} c\kappa_\nu E_\nu\,\mathrm{d}\nu = cE_\omega \left(\frac{1}{|g_\omega|} \int_{\nu_{\omega,L}}^{\nu_{\omega,R}} \kappa_\nu\,\mathrm{d}\nu \right) \equiv cE_\omega \kappa_\omega, \tag{28}$$

where the equations (27) and (28) above define the multi-group emissivities and opacities, η_ω and κ_ω, $\omega = 1, \ldots, N_f$, respectively.

To compute the group opacity κ_ω from equation (28) above, we insert the definition of the chemistry-dependent opacity (5),

$$\kappa_\omega \;=\; \frac{1}{|g_\omega|}\int_{\nu_{\omega,L}}^{\nu_{\omega,R}} \sum_{i=1}^{N_{\rm chem}} \sigma_i(\nu)\,\mathtt{n}_i\,\mathrm{d}\nu \;=\; \sum_{i=1}^{N_{\rm chem}} \mathtt{n}_i \left(\frac{1}{|g_\omega|}\int_{\nu_{\omega,L}}^{\nu_{\omega,R}} \sigma_i(\nu)\,\mathrm{d}\nu\right), \tag{29}$$

which requires integration of the species cross-sections $\sigma_i(\nu)$ over each group's frequency range.

The remaining frequency coupling term is less trivial,

$$\begin{aligned}\frac{\nu\dot{a}}{a}\partial_\nu E_\nu \;\to\; \int_{\nu_{\omega,L}}^{\nu_{\omega,R}} \frac{\nu\dot{a}}{a}\partial_\nu E_\nu\,\mathrm{d}\nu &= \frac{\dot{a}}{a}\int_{\nu_{\omega,L}}^{\nu_{\omega,R}} \nu\,\partial_\nu E_\nu\,\mathrm{d}\nu \\ &= \frac{\dot{a}}{a}\left[(\nu\,E_\nu)\Big|_{\nu_{\omega,L}}^{\nu_{\omega,R}} - \int_{\nu_{\omega,L}}^{\nu_{\omega,R}} E_\nu\,\mathrm{d}\nu\right] \\ &\approx \frac{\dot{a}\,\nu_{\omega,R}}{2a}\left(\frac{E_\omega}{|g_\omega|}+\frac{E_{\omega+1}}{|g_{\omega+1}|}\right) - \frac{\dot{a}\,\nu_{\omega,L}}{2a}\left(\frac{E_{\omega-1}}{|g_{\omega-1}|}+\frac{E_\omega}{|g_\omega|}\right) - \frac{\dot{a}}{a}E_\omega.\end{aligned} \tag{30}$$

We note that derivation of the above term required integration by parts, as well as approximation of the radiation energy density at the bin frequency boundaries,

$$E_\nu(\nu_\omega) \approx \frac{1}{2}\left(\frac{E_{\omega-1}}{|g_{\omega-1}|}+\frac{E_\omega}{|g_\omega|}\right), \qquad E_\nu(\nu_{\omega+1}) \approx \frac{1}{2}\left(\frac{E_\omega}{|g_\omega|}+\frac{E_{\omega+1}}{|g_{\omega+1}|}\right),$$

which is only valid if the radiation groups $E_{\omega-1}$, E_ω and $E_{\omega+1}$ are defined over contiguous bands, i.e. if

$$\nu_{\omega-1,R} = \nu_{\omega,L} \quad \text{and} \quad \nu_{\omega,R} = \nu_{\omega+1,L}. \tag{31}$$

Furthermore, this term accounts for redshifting effects due to cosmological expansion, that pull radiation from higher frequencies downward. Although our multi-group radiation approximation is no longer continuous as a function of frequency, rendering the partial derivative $\partial_\nu E_\nu$ undefined, we have used integration by parts to instead consider this term as a radiation flux from higher-frequency groups downward. In addition, the first and last radiation groups deserve special attention since they cannot have left and right neighbors, respectively (as well as any other groups that have a non-contiguous frequency band with a lower/higher group). For these two groups, we instead approximate

$$\int_{\nu_{1,L}}^{\nu_{1,R}} \frac{\nu\dot{a}}{a}\partial_\nu E_\nu\,\mathrm{d}\nu \approx \frac{\dot{a}\,\nu_{1,R}}{2a}\left(\frac{E_1}{|g_1|}+\frac{E_2}{|g_2|}\right) - \frac{\dot{a}\,\nu_{1,L}E_1}{a|g_1|} - \frac{\dot{a}}{a}E_1, \tag{32}$$

$$\int_{\nu_{N_f,L}}^{\nu_{N_f,R}} \frac{\nu\dot{a}}{a}\partial_\nu E_\nu\,\mathrm{d}\nu \approx \frac{\dot{a}\,\nu_{N_f,R}E_{N_f}}{a|g_{N_f}|} - \frac{\dot{a}\,\nu_{N_f,L}}{2a}\left(\frac{E_{N_f-1}}{|g_{N_f-1}|}+\frac{E_{N_f}}{|g_{N_f}|}\right) - \frac{\dot{a}}{a}E_{N_f}. \tag{33}$$

We note that for intermediate radiation groups whose frequency bands do not touch their "neighbor", we use similar formulas. Similarly, for isolated radiation groups that have no "neighbors", we instead approximate this term as

$$\int_{\nu_{\omega,L}}^{\nu_{\omega,R}} \frac{\nu\dot{a}}{a}\partial_\nu E_\nu\,\mathrm{d}\nu \approx \frac{\dot{a}\,\nu_{\omega,R}\,E_\omega}{a|g_\omega|} - \frac{\dot{a}\,\nu_{\omega,L}\,E_\omega}{a|g_\omega|} - \frac{\dot{a}}{a}E_\omega. \tag{34}$$

Combining all of the above terms, (24)-(34), our multi-group radiation energy density equations may be written as

$$\partial_t E_\omega - \nabla\cdot(D_\omega\,\nabla E_\omega) + \frac{3\dot{a}}{a}E_\omega - (\Diamond) = \eta_\omega - c\kappa_\omega E_\omega, \quad \omega = 0,\ldots,N_f-1, \tag{35}$$

where $(\Diamond)$ corresponds to one of (30), (32), (33) or (34), depending on the contiguity of the frequency bands surround g_ω.

To complete the model, we must determine the photo-heating and photo-ionization terms that couple the radiation to the matter. As before, we utilize the integral form of their definitions, along with the piecewise-constant definition of our radiation energy density (23).

First, we compute the integrated photoionization rate Γ_i^{ph} for each species $\mathtt{n}_i$ as

$$\begin{aligned}\Gamma_i^{ph}(t,\mathbf{r}) &= c\int_{\bar{\nu}_i}^{\infty} \frac{\sigma_{\mathtt{n}_i}(\nu)E_\nu(t,\mathbf{r},\nu)}{h\nu}\,\mathrm{d}\nu = c\sum_{\omega=1}^{N_f}\int_{\nu_{\omega,L}}^{\nu_{\omega,R}} \frac{\sigma_{\mathtt{n}_i}(\nu)E_\omega(t,\mathbf{r})}{h\nu|g_\omega|}\,\mathrm{d}\nu \\ &= \sum_{\omega=1}^{N_f}\frac{cE_\omega(t,\mathbf{r})}{h}\left(\frac{1}{|g_\omega|}\int_{\nu_{\omega,L}}^{\nu_{\omega,R}}\frac{\sigma_{\mathtt{n}_i}(\nu)}{\nu}\,\mathrm{d}\nu\right), \qquad i=1,\ldots,N_{\mathrm{chem}},\end{aligned} \tag{36}$$

where as with the multi-frequency model, we assume that the species cross sections satisfy $\sigma_{\mathtt{n}_i}(\nu)=0$ for all $\nu<\bar{\nu}_i$.

Similarly, we compute the specific photoheating rate as

$$\begin{aligned}G(t,\mathbf{r}) &= \frac{c}{\rho_b}\sum_{i=1}^{N_{\mathrm{chem}}}\mathtt{n}_i\int_{\bar{\nu}_i}^{\infty}\sigma_{\mathtt{n}_i}(\nu)E_\nu(t,\mathbf{r},\nu)\left(\frac{h\nu-h\bar{\nu}_i}{h\nu}\right)\mathrm{d}\nu \\ &= \sum_{i=1}^{N_{\mathrm{chem}}}\sum_{\omega=1}^{N_f}\frac{c\,\mathtt{n}_i\,E_\omega(t,\mathbf{r})}{\rho_b}\left(\frac{1}{|g_\omega|}\int_{\nu_{\omega,L}}^{\nu_{\omega,R}}\sigma_{\mathtt{n}_i}(\nu)\left(1-\frac{\bar{\nu}_i}{\nu}\right)\mathrm{d}\nu\right).\end{aligned} \tag{37}$$

We note that in the formulas (29), (36) and (37), we have the integrals

$$\frac{1}{|g_\omega|}\int_{\nu_{\omega,L}}^{\nu_{\omega,R}}\sigma_{\mathtt{n}_i}(\nu)\,\mathrm{d}\nu, \qquad \frac{1}{|g_\omega|}\int_{\nu_{\omega,L}}^{\nu_{\omega,R}}\frac{\sigma_{\mathtt{n}_i}(\nu)}{\nu}\,\mathrm{d}\nu \qquad \text{and} \qquad \frac{1}{|g_\omega|}\int_{\nu_{\omega,L}}^{\nu_{\omega,R}}\sigma_{\mathtt{n}_i}(\nu)\left(1-\frac{\bar{\nu}_i}{\nu}\right)\mathrm{d}\nu. \tag{38}$$

Since these integrals depend only on the *a-priori* defined radiation groups $g_\omega=[\nu_{\omega,L},\nu_{\omega,R})$ and species cross-sections $\sigma_{\mathtt{n}_i}$, we may compute these once at problem initialization and reuse them throughout the simulation. For each of these integrals, we use an adaptive, high-order Gaussian quadrature method for numerically approximating each integral, manually adjusting any interval bounds to account for regions where $\sigma_i(\nu)=0$.

2 Units in Enzo cosmology

When run with cosmological expansion enabled, Enzo modifies the units of each internal field throughout the simulation to account for cosmological expansion. We define the comoving position $\mathbf{x}$ through the relationship $\mathbf{r}=l_{\mathrm{unit}}\mathbf{x}\propto a\mathbf{x}$ (specific details are below in equation (42)), where a is the cosmological expansion factor. This is a time-dependent (equivalently, redshift-dependent) factor, satisfying the relationship

$$z=\frac{1}{a}-1, \tag{39}$$

where z is the current (time-dependent) redshift. We note that since z decreases as time proceeds, a increases as a function of time, since

$$a=\frac{1}{1+z}. \tag{40}$$

Enzo then defines the unit non-dimensionalization factors:

$$\rho_{\rm unit} = (1.88 \times 10^{-29})\Omega_{mn} H_{cn}^2 (1+z)^3, \tag{41}$$

$$l_{\rm unit} = \frac{(3.086 \times 10^{24}) L_c}{H_{cn}(1+z)} \qquad \left(\text{i.e.} \quad l_{\rm unit} = \frac{(3.086 \times 10^{24}) L_c}{H_{cn}} a\right), \tag{42}$$

$$t_{\rm unit} = \frac{2.52 \times 10^{17}}{\Omega_{mn}^{1/2} H_{cn} (1+z_I)^{3/2}}, \tag{43}$$

$$v_{\rm unit} = (1.225 \times 10^7) L_c \sqrt{\Omega_{mn}(1+z_I)}, \tag{44}$$

$$a_{\rm unit} = (1+z_I)^{-1}. \tag{45}$$

Here $a = a_{\rm unit}\tilde{a}$, where $\tilde{a}$ is Enzo's normalized value, Ω_{mn} is Enzo's `OmegaMatterNow` parameter, H_{cn} is Enzo's `HubbleConstantNow` parameter, z_I is Enzo's `InitialRedshift` parameter, and L_c is Enzo's `ComovingBoxSize` parameter. As a result, Enzo actually computes the current redshift via the formula

$$z = \frac{1+z_I}{\tilde{a}} - 1. \tag{46}$$

We note that under these definitions, $v_{\rm unit} \neq l_{\rm unit}/t_{\rm unit}$, since

$$\begin{aligned} \frac{l_{\rm unit}}{t_{\rm unit}} &= \frac{(3.086 \times 10^{24}) L_c \left(\Omega_{mn}^{1/2} H_{cn} (1+z_I)^{3/2}\right)}{H_{cn}(1+z)\,(2.52 \times 10^{17})} \\ &= (1.2246 \times 10^7) L_c \sqrt{\Omega_{mn}(1+z_I)} \frac{(1+z_I)}{(1+z)}, \end{aligned}$$

which differs from $v_{\rm unit}$ both in the precision of the leading constant (minor difference) and also by a factor of $(1+z_I)/(1+z)$, that grows in magnitude as time proceeds, especially for simulations having large initial redshift (major difference).

With these unit normalization factors defined, we may also consider a unit normalization factor for radiation energy density, that can be defined as either

$$\rho_{\rm unit} v_{\rm unit}^2, \quad \text{or} \quad \rho_{\rm unit} \frac{l_{\rm unit}^2}{t_{\rm unit}^2},$$

since both constitute the correct CGS units. However, since in cosmological simulations $v_{\rm unit} \neq l_{\rm unit}/t_{\rm unit}$, these two definitions are not the same. We choose the first of these,

$$E_{\rm unit} = \rho_{\rm unit} v_{\rm unit}^2. \tag{47}$$

We note that even when run without cosmology, unit scaling factors may be defined within Enzo for running a simulation. In this case, we similarly use Enzo's internal unit scaling factors to define the radiation unit scaling factor, $E_{\rm unit}$.

3 Recasting to comoving, normalized form

Our equations (15), (35) and (11)-(12) are valid in proper CGS units, whereas Enzo's fields are stored in comoving, normalized form. Specifically, the terms in our equations relate to Enzo's comoving, normalized terms in the following manner:

- $\rho_b = \rho_{\rm unit}\tilde{\rho}_b$, where ρ_b is the proper, CGS density, and $\tilde{\rho}_b$ is Enzo's comoving, normalized density value,
- $\mathbf{v}_b = v_{\rm unit}\tilde{\mathbf{v}}_b$, where $\mathbf{v}_b$ is the proper peculiar baryonic CGS velocity, and $\tilde{\mathbf{v}}_b$ is Enzo's comoving, normalized velocity value,

- $e = v_{\rm unit}^2 \tilde{e}$, where e is the proper baryonic energy per unit mass, and $\tilde{e}$ is Enzo's comoving, normalized energy value,
- $E_\omega = E_{\rm unit}\tilde{E}$, where E_ω is the proper, CGS radiation energy (monochromatic or group), and $\tilde{E}_\omega$ is Enzo's comoving, normalized radiation energy value for the specified frequency or group,
- $a = a_{\rm unit}\tilde{a}$, as described above in equation (45),
- $\dot{a} = (a_{\rm unit}/t_{\rm unit})\,\dot{\tilde{a}}$, where $\dot{a}$ is the true cosmological expansion rate, and $\dot{\tilde{a}}$ is Enzo's normalized value,
- $\mathbf{r} = l_{\rm unit}\mathbf{x}$, where $\mathbf{r}$ is the proper, CGS position, and $\mathbf{x}$ is Enzo's comoving normalized position,
- $t = t_{\rm unit}\tilde{t}$, where t is the CGS time, and $\tilde{t}$ is Enzo's normalized time,
- $\kappa_\omega = \tilde{\kappa}_\omega \kappa_{\rm unit}$, where κ_ω is the proper, CGS opacity for the ω-th frequency or group, $\tilde{\kappa}_\omega$ is Enzo's normalized value, and $\kappa_{\rm unit} \propto l_{\rm unit}^{-1}$.

We also note that in order for us to convert our equations for the proper CGS radiation energy (E_ω) to the normalized, comoving radiation energy density ($\tilde{E}_\omega$) we must consider how our time derivative must be modified. Specifically, since $E_\omega = E_{\rm unit}\tilde{E}_\omega$, then by the product rule,

$$\partial_t E_\omega = \partial_t\left(E_{\rm unit}\tilde{E}_\omega\right) = E_{\rm unit}\,\partial_t\tilde{E}_\omega + \tilde{E}_\omega\,\partial_t E_{\rm unit}.$$

Due to our choice of $E_{\rm unit} = \rho_{\rm unit} v_{\rm unit}^2 \propto (1+z)^3$, we then have

$$\partial_t E_{\rm unit} = \frac{3\,E_{\rm unit}\,\partial_t z}{1+z}.$$

Moreover, because $z = \frac{1}{a} - 1$ we have $\partial_t z = -\frac{\dot{a}}{a^2}$, and since $a = \frac{1}{1+z}$, this becomes

$$\partial_t E_{\rm unit} = -3E_{\rm unit}\frac{\dot{a}}{a}.$$

As a result, we have

$$\begin{aligned}\partial_t E_\omega &= E_{\rm unit}\,\partial_t\tilde{E}_\omega - 3E_{\rm unit}\frac{\dot{a}}{a}\tilde{E}_\omega \\ &= E_{\rm unit}\,\partial_t\tilde{E}_\omega - 3\frac{\dot{a}}{a}E_\omega,\end{aligned}$$

which will cancel the term $3\frac{\dot{a}}{a}E_\omega$ in either of the equations (15) or (35). Specifically, after dividing through by $E_{\rm unit}$ and canceling like terms, the multi-frequency equation (15) may instead be written in terms of the comoving, normalized radiation energy density:

$$\partial_t\tilde{E}_\omega - \nabla\cdot(D_\omega\,\nabla\tilde{E}_\omega) + \frac{\dot{a}}{a}\tilde{E}_\omega = \frac{\eta_\omega}{E_{\rm unit}} - c\kappa_\omega\tilde{E}_\omega, \qquad \omega = 0,\ldots,N_f. \tag{48}$$

Similarly, the multi-group equation (35) can be written in comoving, normalized for as:

$$\partial_t\tilde{E}_\omega - \nabla\cdot(D_\omega\,\nabla\tilde{E}_\omega) - (\square)_\omega = \frac{\eta_\omega}{E_{\rm unit}} - c\kappa_\omega\tilde{E}_\omega, \quad \omega = 0,\ldots,N_f-1, \tag{49}$$

where we now define $(\square)_\omega$ as

$$(\square)_\omega = \begin{cases} \frac{\dot{a}\,\nu_{\omega,R}}{2a}\left(\frac{\tilde{E}_\omega}{|g_\omega|} + \frac{\tilde{E}_{\omega+1}}{|g_{\omega+1}|}\right) - \frac{\dot{a}\,\nu_{\omega,L}}{2a}\left(\frac{\tilde{E}_{\omega-1}}{|g_{\omega-1}|} + \frac{\tilde{E}_\omega}{|g_\omega|}\right) - \frac{\dot{a}}{a}\tilde{E}_\omega, & \text{if} \quad \nu_{\omega-1,R} = \nu_{\omega,L},\ \nu_{\omega,R} = \nu_{\omega+1,L}, \\ \frac{\dot{a}\,\nu_{\omega,R}\,\tilde{E}_\omega}{a\,|g_\omega|} - \frac{\dot{a}\,\nu_{\omega,L}}{2a}\left(\frac{\tilde{E}_{\omega-1}}{|g_{\omega-1}|} + \frac{\tilde{E}_\omega}{|g_\omega|}\right) - \frac{\dot{a}}{a}\tilde{E}_\omega, & \text{if} \quad \nu_{\omega-1,R} = \nu_{\omega,L},\ \nu_{\omega,R} \neq \nu_{\omega+1,L}, \\ \frac{\dot{a}\,\nu_{\omega,R}}{2a}\left(\frac{\tilde{E}_\omega}{|g_\omega|} + \frac{\tilde{E}_{\omega+1}}{|g_{\omega+1}|}\right) - \frac{\dot{a}\,\nu_{\omega,L}\,\tilde{E}_\omega}{a\,|g_\omega|} - \frac{\dot{a}}{a}\tilde{E}_\omega, & \text{if} \quad \nu_{\omega-1,R} \neq \nu_{\omega,L},\ \nu_{\omega,R} = \nu_{\omega+1,L}, \\ \frac{\dot{a}\,\tilde{E}_\omega}{a\,|g_\omega|}\left(\nu_{\omega,R} - \nu_{\omega,L}\right) - \frac{\dot{a}}{a}\tilde{E}_\omega = 0, & \text{if} \quad \nu_{\omega-1,R} \neq \nu_{\omega,L},\ \nu_{\omega,R} \neq \nu_{\omega+1,L}. \end{cases} \tag{50}$$

Similarly, since the proper position changes as a function of time, then we may consider spatial differentiation with respect to the normalized comoving position $\mathbf{x}$. Since

$$\mathbf{r} = l_{\rm unit}\mathbf{x} \quad \Longleftrightarrow \quad \mathbf{x} = \frac{\mathbf{r}}{l_{\rm unit}},$$

then the chain rule dictates that

$$\frac{\partial}{\partial \mathbf{r}} \;=\; \frac{\partial \mathbf{x}}{\partial \mathbf{r}}\frac{\partial}{\partial \mathbf{x}} \;=\; \frac{1}{l_{\rm unit}}\frac{\partial}{\partial \mathbf{x}}.$$

We therefore denote the comoving, normalized differentiation operator as $\tilde{\nabla}$, such that

$$\nabla = \frac{1}{l_{\rm unit}}\tilde{\nabla}.$$

Resultingly, upon converting (48) to comoving, normalized units, we have the multi-frequency equation

$$\partial_t \tilde{E}_\omega - \frac{1}{l_{\rm unit}^2}\tilde{\nabla}\cdot\left(D_\omega\,\tilde{\nabla}\tilde{E}_\omega\right) + \frac{\dot{a}}{a}\tilde{E}_\omega = \frac{\eta_\omega}{E_{\rm unit}} - c\kappa_\omega\tilde{E}_\omega, \quad \omega = 0,\ldots,N_f, \tag{51}$$

and converting (49) we obtain the multi-group equation

$$\partial_t \tilde{E}_\omega - \frac{1}{l_{\rm unit}^2}\tilde{\nabla}\cdot(D_\omega\,\tilde{\nabla}\tilde{E}_\omega) - (\Box)_\omega = \frac{\eta_\omega}{E_{\rm unit}} - c\kappa_\omega\tilde{E}_\omega, \quad \omega = 0,\ldots,N_f-1. \tag{52}$$

Similarly, we may consider time differentiation with respect to the normalized time value, $\tilde{t}$:

$$\frac{\partial}{\partial t} \;=\; \frac{\partial \tilde{t}}{\partial t}\frac{\partial}{\partial \tilde{t}} \;=\; \frac{1}{t_{\rm unit}}\frac{\partial}{\partial \tilde{t}}.$$

Inserting this into (51) we have the multi-frequency equations

$$\partial_{\tilde{t}} \tilde{E}_\omega - \frac{t_{\rm unit}}{l_{\rm unit}^2}\tilde{\nabla}\cdot\left(D_\omega\,\tilde{\nabla}\tilde{E}_\omega\right) + \frac{t_{\rm unit}\,\dot{a}}{a}\tilde{E}_\omega = \frac{t_{\rm unit}\eta_\omega}{E_{\rm unit}} - t_{\rm unit}c\kappa_\omega\tilde{E}_\omega, \quad \omega = 0,\ldots,N_f, \tag{53}$$

and inserting into (52) we have the corresponding multi-group version,

$$\partial_{\tilde{t}} \tilde{E}_\omega - \frac{t_{\rm unit}}{l_{\rm unit}^2}\tilde{\nabla}\cdot(D_\omega\,\tilde{\nabla}\tilde{E}_\omega) - t_{\rm unit}(\Box)_\omega = \frac{t_{\rm unit}\eta_\omega}{E_{\rm unit}} - t_{\rm unit}c\kappa_\omega\tilde{E}_\omega, \quad \omega = 0,\ldots,N_f-1. \tag{54}$$

Lastly, we will convert these equations so that they depend only on Enzo's normalized variables, $\tilde{t}$, $\tilde{E}_\omega$, $\tilde{a}$, $\dot{\tilde{a}}$ and $\tilde{\kappa}_\omega$. To this end, we expand each variable in terms of its normalized value and unit factor. We begin with the multi-frequency equations:

$$\partial_{\tilde{t}} \tilde{E}_\omega - \frac{t_{\rm unit}}{l_{\rm unit}^2}\tilde{\nabla}\cdot\left(D_\omega\,\tilde{\nabla}\tilde{E}_\omega\right) + \frac{t_{\rm unit}\,\dot{\tilde{a}}\,a_{\rm unit}}{t_{\rm unit}\,\tilde{a}\,a_{\rm unit}}\tilde{E}_\omega = \frac{t_{\rm unit}\,\eta_\omega}{E_{\rm unit}} - t_{\rm unit}\,\kappa_{\rm unit}\,c\,\tilde{\kappa}_\omega\,\tilde{E}_\omega, \quad \omega = 0,\ldots,N_f,$$

$$\Leftrightarrow \tag{55}$$

$$\partial_{\tilde{t}} \tilde{E}_\omega - \frac{t_{\rm unit}}{l_{\rm unit}^2}\tilde{\nabla}\cdot\left(D_\omega\,\tilde{\nabla}\tilde{E}_\omega\right) + \frac{\dot{\tilde{a}}}{\tilde{a}}\tilde{E}_\omega = \frac{t_{\rm unit}\,\eta_\omega}{E_{\rm unit}} - t_{\rm unit}\,\kappa_{\rm unit}\,c\,\tilde{\kappa}_\omega\,\tilde{E}_\omega, \quad \omega = 0,\ldots,N_f, \tag{56}$$

where we compute the limiter as

$$D_{\omega,i} = c\left(9\tilde{\kappa}_\omega^2\kappa_{\rm unit}^2 + R_{\omega,i}^2\right)^{-1/2}, \quad i = 1,2,3, \quad \omega = 0,\ldots,N_f \tag{57}$$

$$R_{\omega,i} = \frac{|\partial_{\mathbf{x}_i}\tilde{E}_\omega|}{l_{\rm unit}\tilde{E}_\omega}, \quad i = 1,2,3, \quad \omega = 0,\ldots,N_f. \tag{58}$$

Similarly, for the multi-group equations, we have for each $\omega = 0, \ldots, N_f - 1$,

$$\partial_{\tilde{t}} \tilde{E}_\omega - \frac{t_{\rm unit}}{l_{\rm unit}^2} \tilde{\nabla} \cdot \left(D_\omega \, \tilde{\nabla} \tilde{E}_\omega \right) - t_{\rm unit} (\Box)_\omega = \frac{t_{\rm unit} \eta_\omega}{E_{\rm unit}} - t_{\rm unit} \, \kappa_{\rm unit} \, c \, \tilde{\kappa}_\omega \, \tilde{E}_\omega,$$

$$\Leftrightarrow \tag{59}$$

$$\partial_{\tilde{t}} \tilde{E}_\omega - \frac{t_{\rm unit}}{l_{\rm unit}^2} \tilde{\nabla} \cdot \left(D_\omega \, \tilde{\nabla} \tilde{E}_\omega \right) - (\tilde{\Box})_\omega = \frac{t_{\rm unit} \eta_\omega}{E_{\rm unit}} - t_{\rm unit} \, \kappa_{\rm unit} c \, \tilde{\kappa}_\omega \, \tilde{E}_\omega, \tag{60}$$

with the limiter the same as in (57)-(58), and where we compute $(\tilde{\Box})_\omega$ as

$$(\tilde{\Box})_\omega = \begin{cases} \frac{\tilde{\dot{a}} \, \nu_{\omega,R}}{2\tilde{a}} \left(\frac{\tilde{E}_\omega}{|g_\omega|} + \frac{\tilde{E}_{\omega+1}}{|g_{\omega+1}|} \right) - \frac{\tilde{\dot{a}} \, \nu_{\omega,L}}{2\tilde{a}} \left(\frac{\tilde{E}_{\omega-1}}{|g_{\omega-1}|} + \frac{\tilde{E}_\omega}{|g_\omega|} \right) - \frac{\tilde{\dot{a}}}{\tilde{a}} \tilde{E}_\omega, & \text{if} \quad \nu_{\omega-1,R} = \nu_{\omega,L}, \; \nu_{\omega,R} = \nu_{\omega+1,L}, \\ \frac{\tilde{\dot{a}} \, \nu_{\omega,R} \, \tilde{E}_\omega}{\tilde{a} \, |g_\omega|} - \frac{\tilde{\dot{a}} \, \nu_{\omega,L}}{2\tilde{a}} \left(\frac{\tilde{E}_{\omega-1}}{|g_{\omega-1}|} + \frac{\tilde{E}_\omega}{|g_\omega|} \right) - \frac{\tilde{\dot{a}}}{\tilde{a}} \tilde{E}_\omega, & \text{if} \quad \nu_{\omega-1,R} = \nu_{\omega,L}, \; \nu_{\omega,R} \neq \nu_{\omega+1,L}, \\ \frac{\tilde{\dot{a}} \, \nu_{\omega,R}}{2\tilde{a}} \left(\frac{\tilde{E}_\omega}{|g_\omega|} + \frac{\tilde{E}_{\omega+1}}{|g_{\omega+1}|} \right) - \frac{\tilde{\dot{a}} \, \nu_{\omega,L} \, \tilde{E}_\omega}{\tilde{a} \, |g_\omega|} - \frac{\tilde{\dot{a}}}{\tilde{a}} \tilde{E}_\omega, & \text{if} \quad \nu_{\omega-1,R} \neq \nu_{\omega,L}, \; \nu_{\omega,R} = \nu_{\omega+1,L}, \\ 0, & \text{if} \quad \nu_{\omega-1,R} \neq \nu_{\omega,L}, \; \nu_{\omega,R} \neq \nu_{\omega+1,L}. \end{cases} \tag{61}$$

4 Finite volume PDE approximation

We define the spatially-discretized version of our equations in the context of a uniform (i.e. non-AMR) mesh with comoving grid spacings Δx, Δy and Δz; as the AMR extensions of this involve a standard extension of the same equation over patches with smaller mesh size, the uniform grid assumption will prove sufficient for this derivation. On this uniform grid, we define the finite volume cell centers at the grid points in comoving, normalized units as:

$$\begin{aligned} \mathbf{x}_{i,j,k} &= [\, x_i, \, y_j, \, z_k \,], \\ x_i &= \left(i + \tfrac{1}{2} \right) \Delta x, \\ y_j &= \left(j + \tfrac{1}{2} \right) \Delta y, \\ z_k &= \left(k + \tfrac{1}{2} \right) \Delta z. \end{aligned}$$

Enzo's data arrays contain the discrete values of each field over the simulation volume at each of these grid points. More specifically, Enzo uses three-dimensional data arrays to store these discretized solution values at specific points in time. We denote $\tilde{E}^n_{\omega,i,j,k}$ as our approximation to the comoving and normalized solution at the normalized time $\tilde{t}_n$ and at the comoving normalized spatial location $\mathbf{x}_{i,j,k}$ (and do similarly for the other field data). We must therefore consider how to discretize the space and time derivatives of our equations (56) and (60) so that they depend on only these discrete data values.

We first separate the space and time discretizations. First, we discretize in time using a one-step θ-method. Introducing the notation

$$\mathcal{D}_\omega(\tilde{E}_\omega, \tilde{\kappa}_\omega, \eta_\omega, \tilde{a}, \tilde{\dot{a}}) = \frac{t_{\rm unit}}{l_{\rm unit}^2} \tilde{\nabla} \cdot \left(D_\omega \, \tilde{\nabla} \tilde{E}_\omega \right) - \frac{\tilde{\dot{a}}}{\tilde{a}} \tilde{E}_\omega + \frac{t_{\rm unit} \eta_\omega}{E_{\rm unit}} - t_{\rm unit} \kappa_{\rm unit} \, c \, \tilde{\kappa}_\omega \, \tilde{E}_\omega$$

for the multi-frequency equation (56), or

$$\mathcal{D}_\omega(\tilde{E}_\omega, \tilde{\kappa}_\omega, \eta_\omega, \tilde{a}, \tilde{\dot{a}}) = \frac{t_{\rm unit}}{l_{\rm unit}^2} \tilde{\nabla} \cdot \left(D_\omega \, \tilde{\nabla} \tilde{E}_\omega \right) + (\tilde{\Box})_\omega + \frac{t_{\rm unit} \eta_\omega}{E_{\rm unit}} - t_{\rm unit} \kappa_{\rm unit} \, c \, \tilde{\kappa}_\omega \, \tilde{E}_\omega$$

for the multi-group equation (60), and denoting $\tilde{E}^n_\omega$ as our approximation to the spatially continuous solution at time $\tilde{t}_n$, the θ-method for both equations (56) and (60) may be written as

$$\tilde{E}^{n+1}_\omega - \tilde{E}^n_\omega = \theta \Delta \tilde{t} \mathcal{D}(\tilde{E}^{n+1}_\omega, \tilde{\kappa}^{n+1}_\omega, \eta^{n+1}_\omega, \tilde{a}^{n+1}, \tilde{\dot{a}}^{n+1}) + (1-\theta) \Delta \tilde{t} \mathcal{D}(\tilde{E}^n_\omega, \tilde{\kappa}^n_\omega, \eta^n_\omega, \tilde{a}^n, \tilde{\dot{a}}^n), \tag{62}$$

where in the first $\mathcal{D}$ term we lag the implicit dependence of the solution on the flux limiter D_ω^{n+1} to the previous time, D_ω^n to result in a linearly implicit system of equations. Furthermore, to decouple the linear systems for each radiation field, we also lag the implicit dependence on the redshifting term $(\tilde{\square})_\omega^{n+1}$ to the previous time, $(\tilde{\square})_\omega^n$. We note that although these approximations limit the asymptotic convergence rate of any θ-method to first-order in time, i.e. $\mathcal{O}(\Delta t)$, these do not affect energy conservation since the spatial fluxes use consistent values of D_ω^n, and the frequency fluxes use consistent values of $(\tilde{\square})_\omega^n$.

We must similarly apply our finite-volume spatial discretization of the operator $\mathcal{D}_\omega$. For the discretized equation for frequency/group ω, centered at the comoving normalized spatial position $\mathbf{x}_{i,j,k}$, we have

$$\tilde{E}^{n+1}_{\omega,i,j,k} - \tilde{E}^{n}_{\omega,i,j,k} = \theta\Delta\tilde{t}\mathcal{D}^{n+1}_{\omega,i,j,k} + (1-\theta)\Delta\tilde{t}\mathcal{D}^{n}_{\omega,i,j,k}, \tag{63}$$

where for the multi-frequency equations

$$\begin{aligned}
\mathcal{D}_{\omega,i,j,k} = &\frac{t_{\text{unit}}}{l_{\text{unit}}^2\Delta x^2}\left(D_{\omega,i+1/2,j,k}\left(\tilde{E}_{\omega,i+1,j,k}-\tilde{E}_{\omega,i,j,k}\right) - D_{\omega,i-1/2,j,k}\left(\tilde{E}_{\omega,i,j,k}-\tilde{E}_{\omega,i-1,j,k}\right)\right) \\
&+ \frac{t_{\text{unit}}}{l_{\text{unit}}^2\Delta y^2}\left(D_{\omega,i,j+1/2,k}\left(\tilde{E}_{\omega,i,j+1,k}-\tilde{E}_{\omega,i,j,k}\right) - D_{\omega,i,j-1/2,k}\left(\tilde{E}_{\omega,i,j,k}-\tilde{E}_{\omega,i,j-1,k}\right)\right) \\
&+ \frac{t_{\text{unit}}}{l_{\text{unit}}^2\Delta z^2}\left(D_{\omega,i,j,k+1/2}\left(\tilde{E}_{\omega,i,j,k+1}-\tilde{E}_{\omega,i,j,k}\right) - D_{\omega,i,j,k-1/2}\left(\tilde{E}_{\omega,i,j,k}-\tilde{E}_{\omega,i,j,k-1}\right)\right) \\
&- \frac{\tilde{\dot{a}}}{\tilde{a}}\tilde{E}_{\omega,i,j,k} + \frac{t_{\text{unit}}\eta_{\omega,i,j,k}}{E_{\text{unit}}} - t_{\text{unit}}\kappa_{\text{unit}}\, c\,\tilde{\kappa}_{\omega,i,j,k}\tilde{E}_{\omega,i,j,k},
\end{aligned} \tag{64}$$

and for the multi-group equations

$$\begin{aligned}
\mathcal{D}_{\omega,i,j,k} = &\frac{t_{\text{unit}}}{l_{\text{unit}}^2\Delta x^2}\left(D_{\omega,i+1/2,j,k}\left(\tilde{E}_{\omega,i+1,j,k}-\tilde{E}_{\omega,i,j,k}\right) - D_{\omega,i-1/2,j,k}\left(\tilde{E}_{\omega,i,j,k}-\tilde{E}_{\omega,i-1,j,k}\right)\right) \\
&+ \frac{t_{\text{unit}}}{l_{\text{unit}}^2\Delta y^2}\left(D_{\omega,i,j+1/2,k}\left(\tilde{E}_{\omega,i,j+1,k}-\tilde{E}_{\omega,i,j,k}\right) - D_{\omega,i,j-1/2,k}\left(\tilde{E}_{\omega,i,j,k}-\tilde{E}_{\omega,i,j-1,k}\right)\right) \\
&+ \frac{t_{\text{unit}}}{l_{\text{unit}}^2\Delta z^2}\left(D_{\omega,i,j,k+1/2}\left(\tilde{E}_{\omega,i,j,k+1}-\tilde{E}_{\omega,i,j,k}\right) - D_{\omega,i,j,k-1/2}\left(\tilde{E}_{\omega,i,j,k}-\tilde{E}_{\omega,i,j,k-1}\right)\right) \\
&+ (\tilde{\square})_{\omega,i,j,k} + \frac{t_{\text{unit}}\eta_{\omega,i,j,k}}{E_{\text{unit}}} - t_{\text{unit}}\kappa_{\text{unit}}\, c\,\tilde{\kappa}_{\omega,i,j,k}\tilde{E}_{\omega,i,j,k},
\end{aligned} \tag{65}$$

with

$$(\tilde{\square})_{\omega,i,j,k} = \begin{cases}
\frac{\tilde{\dot{a}}\,\nu_{\omega,R}}{2\tilde{a}}\left(\frac{\tilde{E}_{\omega,i,j,k}}{|g_\omega|}+\frac{\tilde{E}_{\omega+1,i,j,k}}{|g_{\omega+1}|}\right) - \frac{\tilde{\dot{a}}\,\nu_{\omega,L}}{2\tilde{a}}\left(\frac{\tilde{E}_{\omega-1,i,j,k}}{|g_{\omega-1}|}+\frac{\tilde{E}_{\omega,i,j,k}}{|g_\omega|}\right) - \frac{\tilde{\dot{a}}}{\tilde{a}}\tilde{E}_{\omega,i,j,k}, & \text{if (a)}, \\
\frac{\tilde{\dot{a}}\,\nu_{\omega,R}\,\tilde{E}_{\omega,i,j,k}}{\tilde{a}\,|g_\omega|} - \frac{\tilde{\dot{a}}\,\nu_{\omega,L}}{2\tilde{a}}\left(\frac{\tilde{E}_{\omega-1,i,j,k}}{|g_{\omega-1}|}+\frac{\tilde{E}_{\omega,i,j,k}}{|g_\omega|}\right) - \frac{\tilde{\dot{a}}}{\tilde{a}}\tilde{E}_{\omega,i,j,k}, & \text{if (b)}, \\
\frac{\tilde{\dot{a}}\,\nu_{\omega,R}}{2\tilde{a}}\left(\frac{\tilde{E}_{\omega,i,j,k}}{|g_\omega|}+\frac{\tilde{E}_{\omega+1,i,j,k}}{|g_{\omega+1}|}\right) - \frac{\tilde{\dot{a}}\,\nu_{\omega,L}\,\tilde{E}_{\omega,i,j,k}}{\tilde{a}\,|g_\omega|} - \frac{\tilde{\dot{a}}}{\tilde{a}}\tilde{E}_{\omega,i,j,k}, & \text{if (c)}, \\
0, & \text{if (d)},
\end{cases} \tag{66}$$

where (a) occurs if $\nu_{\omega-1,R} = \nu_{\omega,L},\ \nu_{\omega,R} = \nu_{\omega+1,L}$, (b) occurs if $\nu_{\omega-1,R} = \nu_{\omega,L},\ \nu_{\omega,R} \neq \nu_{\omega+1,L}$, (c) occurs if $\nu_{\omega-1,R} \neq \nu_{\omega,L},\ \nu_{\omega,R} = \nu_{\omega+1,L}$, and (d) occurs if $\nu_{\omega-1,R} \neq \nu_{\omega,L},\ \nu_{\omega,R} \neq \nu_{\omega+1,L}$. In the above, we must discretize the limiter at the faces $\{(i\pm\frac{1}{2},j,k),(i,j\pm\frac{1}{2},k),(i,j,k\pm\frac{1}{2})\}$. Furthermore, due to the limitations of floating-point arithmetic we must enforce bounds on the calculations within the limiter to avoid overflow errors. With these constraints in mind, we discretize the limiter as, e.g.

$$\begin{aligned}
D_{\omega,i+1/2,j,k} &= \min\left\{c\left(9\kappa^2_{\omega,i+1/2,j,k} + R^2_{\omega,i+1/2,j,k}\right)^{-1/2}, D_{\max}\right\}, \\
R_{\omega,i+1/2,j,k} &= \max\left\{\frac{2}{l_{\text{unit}}\Delta x}\frac{|\tilde{E}_{\omega,i+1,j,k}-\tilde{E}_{\omega,i,j,k}|}{\tilde{E}_{\omega,i+1,j,k}+\tilde{E}_{\omega,i,j,k}}, R_{\min}\right\}, \\
\kappa_{\omega,i+1/2,j,k} &= \frac{2\tilde{\kappa}_{\omega,i+1,j,k}\tilde{\kappa}_{\omega,i,j,k}}{\tilde{\kappa}_{\omega,i+1,j,k}+\tilde{\kappa}_{\omega,i,j,k}}\kappa_{\text{unit}}.
\end{aligned} \tag{67}$$

While the limiter formulation shown here is somewhat standard in the field, some of these specific implementation details have proven difficult to master, which we will point out here. First, through significant trial and error, we have found that the limiter bounds $R_{\rm min} = 10^{-2} l_{\rm unit}^{-1}$ and $D_{\rm max} = 10^{-2}\, c\, l_{\rm unit}$ provide the most robust results in a wide range of simulations, including "lab-frame" radiation-hydrodynamics test problems, "medium-scale" astrophysical simulations, and "large-scale" cosmological reionization simulations. The user may over-ride the constants 10^{-2} and 10^{-2} in these definitions if desired, as described in Section 5. Second, we note that the face-centered radiation field ($\tilde{E}_{\omega,i+1/2,j,k}$) and the face-centered opacity ($\kappa_{\omega,i+1/2,j,k}$) are computed differently. In computing the face-centered radiation field (denominator of $R_{\omega,i+1/2,j,k}$) we use the arithmetic mean of the neighboring cell-centered quantities, however in computing the face-centered opacity we use the harmonic mean of the cell-centered quantities. While theoretically both are equally valid, our experience has shown that these approaches give the most robust results in cosmological ionization simulations, wherein opacities may differ by orders of magnitude in neighboring cells.

Furthermore, we note that in many of the above factors from equations (63)-(67), the unit values may change as a function of time due to cosmological expansion. As a result, all quantities are converted using the unit evaluated at the appropriate time step, t_{n+1} or t_n.

We solve the linear systems (63) independently, where each system is solved in predictor-corrector form. We first write the time-evolved solution for a given field as

$$\tilde{E}_\omega^{n+1} = \tilde{E}_p + \delta\tilde{E},$$

where $\tilde{E}_p$ is the predicted solution, and $\delta\tilde{E}$ the the corrector. We then solve the linear system

$$A\delta\tilde{E} = b, \tag{68}$$

where the matrix A corresponds to the linearization

$$A = \frac{\partial}{\partial\tilde{E}_\omega}\left(\tilde{E}_\omega - \theta\Delta\tilde{t}\mathcal{D}_\omega\right)$$

(as previously noted, here both the limiter and redshifting terms are time-lagged), and the right-hand side has the form

$$b = \tilde{E}_\omega^n + (1-\theta)\Delta\tilde{t}\mathcal{D}_{\omega,i,j,k}^n - A\tilde{E}_p^n.$$

For the predictor we use the previous solution, $\tilde{E}_p = \tilde{E}_\omega^n$, and upon solving $A\delta\tilde{E} = b$, we compute $\tilde{E}_\omega^{n+1}$ via

$$\tilde{E}_\omega^{n+1} = \tilde{E}_\omega^n + \delta\tilde{E}.$$

5 Enzo User Interface

In this section we describe the user interface for control over the AMR-FLD solver for Enzo simulations. We begin with description of the supported input parameters, for use of existing AMR-FLD functionality. We follow this with discussion on how to extend the AMR-FLD functionality to admit new physical processes.

5.1 AMR-FLD Input Parameters:

We break apart the basic set of AMR-FLD input parameters into two groups, the first addresses parameters to control the physics performed within the AMR-FLD module, and the second group contains parameters to control the inner-workings of the AMR-FLD solver algorithms themselves.

5.1.1 Physics input parameters

In order to specify how many radiation frequencies and/or groups are desired in a calculation, the following parameter must be included in the AMR-FLD input parameter file:

> `AMRFLDNumRadiationFields` – integer denoting the number of radiation fields, N_f. This value must be non-negative and cannot exceed `MAX_FLD_FIELDS` (stored within `macros_and_parameters.h`, currently 10). Default: 0.

For each of the radiation fields specified above, the user must describe the frequency-space characteristics of each field using the following input parameter:

> `AMRFLDFrequencyBand[:]` – pair of floating-point values denoting the frequency band for the specified radiation group. If the upper limit is less than or equal to the lower limit, then the field is considered monochromatic at the lower bound frequency. For example, to specify three frequency bands: E_0 spans the frequencies 13.6 to 24.4 eV, E_1 is monochromatic at the frequency 54.4 eV, and E_2 is monochromatic at the frequency 100.0 eV, we could use the inputs:
>
> ```
> AMRFLDFrequencyBand[0] = 13.6 24.4
> AMRFLDFrequencyBand[1] = 54.4 54.4
> AMRFLDFrequencyBand[2] = 100.0 99.0
> ```

A user must supply `AMRFLDNumRadiationFields` of these frequency band pairs, and they must be ordered by increasing frequencies (i.e we could not reorder the fields in the above example). Additionally, the fields may not overlap (although neighboring non-monochromatic group bands may share a boundary). The first value specified for each field must be strictly positive.

In order to specify radiation sources for a simulation, the AMR-FLD module provides a simple interface for user specification of sources known at run-time. First, a user must specify the number of radiation sources to be applied with the parameter:

> `AMRFLDNumSources` – integer specifying the number of ionization sources to be specified in the input file (as opposed to on-the-fly by star-maker or other routines). Must be non-negative. Default: 0.

The maximum number of allowed sources is given by `MAX_FLD_SOURCES`, set in `AMRFLDSplit.h` (currently 100).

For each radiation source, AMR-FLD requires knowledge of the source location and how to apply the source to each radiation field. To describe the spatial location of each source, the following parameter must be supplied:

> `AMRFLDSourceLocation[:]` – set of three floating-point values specifying the location of each source (in normalized code units). Must be within the simulation domain.

Each source is assumed to have a "radius" of one cell, meaning that for each source, we scan through the simulation domain, and every computational cell whose center is within one cell of the specified location will receive an equal share of the source's energy.

We have two mechanisms for specifying the emission strength of each source. The first, and more convenient, approach only works for supplying emission to radiation groups (*not* for monochromatic radiation fields). Within this approach, a user must first specify both the *type* of radiation emission using the parameter:

`AMRFLDSourceType[:]` – integer flag denoting a pre-defined SED to use for all emissivity from a given source. Two are currently implemented: 0 indicates a monochromatic source at frequency $h\nu = 13.6$ eV, and 1 indicates a blackbody source having temperature 10^5 K.

If a value is supplied, it *must* correspond to one of the above integers. Additional SED types may be easily defined, as will be described in Section 5.2.

Then, the user must specify the *strength* of the emission source via the parameter:

`AMRFLDSourceEnergy[:]` – floating-point value specifying the total emissivity rate of ionizing photons (i.e. only photons with frequencies above 13.6 eV), for a given source. The value should be specified in units of photon number per second.

Must be used in combination with `AMRFLDSourceType[:]`. At solver initialization, the SED will be numerically integrated over each radiation frequency band $[\nu_i, \nu_{i+1}]$ to determine each group's fraction of the total number of emitted photons for the source. These values are automatically converted into energy emission rates for each source/group. Further details on this process are described in equation (69).

If a value is supplied, it must be non-negative.

If this approach for setting the emission strength of a source is used, both values (`AMRFLDSourceType` and `AMRFLDSourceEnergy`) *must* be specified for each source. We further note that this approach does not make sense unless using a multi-group solver (i.e. not multi-frequency), since the "frequency band" for a monochromatic field by definition has no width. As such, any monochromatic fields in use will be skipped, and will not receive any emissivity from sources described in this manner.

Our second approach for input parameter specification of radiation sources requires the user to manually determine the amount of energy that should be injected into each radiation field. This approach makes use of the parameter:

`AMRFLDSourceGroupEnergy` – floating-point value for the total emissivity rate of ionizing radiation for a specific source over a specific frequency/group (in physical units of ergs s^{-1}). The first index is the source index, the second is the frequency/group index.

We note that this is the only mechanism to specify sources for monochromatic radiation fields via the parameter file.

If a value is supplied, it must be non-negative.

When this approach is used it must specify a non-negative energy value for that source's contribution to *all* radiation fields; i.e. if such a source does not contribute to certain radiation fields, it must specify an `AMRFLDSourceGroupEnergy` of 0.0.

When manually specifying these values for a source with spectral energy distribution $\sigma(\nu)$ and strength $\dot{N}_\gamma$ photons/sec, the correct formula to compute the radiation contribution to a radiation group with frequency band $[\nu_L, \nu_R]$ is

$$h\dot{N}_\gamma \frac{\int_{\nu_L}^{\nu_R} [\nu\sigma(\nu)]\, \mathrm{d}\nu}{\nu_0 \int_{\nu_0}^{\infty} \sigma(\nu)\, \mathrm{d}\nu}, \tag{69}$$

where h is Planck's constant, ν_0 is the ionization threshold of Hydrogen, and all frequency-related values are in units of Hz.

We note that one of these two approaches must be employed for each of the `AMRFLDNumSources` sources. If any of the `AMRFLDNumSources` emission sources is improperly specified, Enzo will return with an error.

Alternately, if *both* approaches are specified for a given source (i.e. both `AMRFLDSourceGroupEnergy` and `AMRFLDSourceType`/`AMRFLDSourceEnergy`), the values provided by `AMRFLDSourceGroupEnergy` are used.

5.1.2 Solver input parameters

We break the set of solver input parameters into four main groups: those that help describe the simulation, those that help control time step adaptivity, and those that control the behavior of the underlying numerical methods. Within these, there are some parameters that we do not recommend users modify unless they are fully aware of their ramifications. These are listed at the end of each group, and are marked by †.

General problem definition:

`AMRFLDRadiationScaling[:]` – scaling factor to be applied to each radiation field to help non-dimensionalize within solver. This is primarily useful if Enzo's default unit normalization factors are insufficient in normalizing the radiation fields. Default: 1.

The easiest way to set this is after performing a test run (preferrably on a coarser mesh), if the "normalized" values for each radiation field do not have unit magnitude, then set this input parameter to be the magnitude of the values resulting from the initial run (we divide by the scaling factor).

`AMRFLDRadiationBoundaryX0` – separate boundary conditions may be applied to the radiation fields than to Enzo's other solution variables. Three types of conditions are currently implemented: 0 periodic, 1 Dirichlet, and 2 Neumann. This input provides a pair of conditions to apply to the lower and upper faces in the first spatial dimension; a pair of integers must be supplied. Default: 0 0.

By default, if the Dirichlet or Neumann boundary condition types are selected, they will use zero-valued (homogeneous) values. Nonzero values may be specified if desired, as discussed in Section 5.2.

`AMRFLDRadiationBoundaryX1` – same as `AMRFLDRadiationBoundaryX1`, but apply in the second spatial dimension.

`AMRFLDRadiationBoundaryX2` – same as `AMRFLDRadiationBoundaryX1`, but apply in the second spatial dimension.

`AMRFLDIsothermal` – flag to denote that all chemistry rates should be frozen to their values at the initial temperature in the lower-left corner of each processor. This is typically used when specifying an initially uniform temperature field, to simulate isothermal test problems. Nonzero values will enable the isothermal model. Default: 0 (off).

`AMRFLDWeakScaling` – flag to denote that all radiation sources specified by the input file should be replicated within each root grid tile. The locations are shifted so that the specified values are given in relation to each root grid tile. This flag is useful for allowing non-trivial emission fields for large weak-scaling tests. Nonzero values will enable the option. Default: 0 (off).

Timestep adaptivity:

`AMRFLDMaxDt` – this parameter sets the maximum normalized time step size allowed within the AMR-FLD solver. Any supplied value must be greater than 0. This value must be given in *scaled*

time units, i.e. $\Delta t_{\rm physical} \le \Delta t_{\rm max} * {\rm TimeUnits}$, where TimeUnits is Enzo's internal time scaling factor for the simulation. Default: 10^{20} (hydro time step size).

`AMRFLDMinDt` – this parameter sets the minimum normalized time step size allowed within the AMR-FLD solver. Any supplied value must be non-negative. This value must also be given in scaled time units. Default: 0 (no minimum).

`AMRFLDInitDt` – this parameter sets the initial normalized time step size for the FLD solver module. Default: ∞ (hydro time step size).

`AMRFLDDtGrowth` – this parameter gives the maximum growth factor in the AMR-FLD time step size from one step to the next. Default: 1.1 (10% growth per step).

`AMRFLDTimeAccuracy` – this parameter gives the maximum desired relative change in the solution from one step to the next. A floor is applied within estimating the relative change to account for the early phases of simulations when the radiation has not built up (or stars have not yet ignited). Any supplied value must be positive. Default: 10^{20} (no accuracy tolerance).

`AMRFLDTheta`† – this parameter determines the value of θ used within equation (62). Typical values are 1 (backward Euler) and 0.5 (trapezoidal or Crank-Nicholson). Default: 1.

`AMRFLDDtControl`† – this parameter controls the time step adaptivity algorithm. Allowed values are -1 (original controller), 0 (I, or "deadbeat" controller), 1 (PI controller), 2 (PID controller). Default: 2.

`AMRFLDDtNorm`† – this parameter dictates the the type of norm used in determining the "relative change" for time step adaptivity. Any supplied value must be non-negative. A value of 0 indicates the maximum or ∞-norm. A value of 2 indicates the standard RMS-norm. Default: 2.

`AMRFLDMaxSubcycles`† – this parameter allows the AMR-FLD solver to subcycle at a faster rate than the hydrodynamics solver. The input value corresponds to the desired number of AMR-FLD steps per hydro step. *Warning: this also further decouples the radiation from the chemistry, which may be a terrible idea since these two processes are intimately coupled through the opacity and photo-ionization.* Default: 1 (no subcycling).

Numerical solver modification:

`AMRFLDSolType` – this integer flag indicates the type of linear solver to use on each radiation system. Allowed values include 0 (FAC), 1 (BiCGStab), 2 (BiCGStab-BoomerAMG), 3 (GMRES), 4 (PFMG, unigrid only). Default: 1.

`AMRFLDSolTolerance` – this floating-point input indicates the desired relative error in solving the linear system (68). Default: 10^{-5}.

`AMRFLDMaxMGIters` – this integer indicates maximum number of outer linear solver iterations taken on each radiation field at each time step. the Default: 200.

`AMRFLDMGRelaxType` – when using the `AMRFLDSolType` 4 (PFMG), this integer parameter indicates the relaxation/smoother algorithm to use in the multigrid cycle. Allowed values include: 0 (Jacobi), 1 (weighted Jacobi), 2 (red-black Gauss-Seidel, symmetric), 3 (red-black Gauss-Seidel, nonsymmetric). Default: 1.

`AMRFLDPreRelax` – when using the `AMRFLDSolType` 4 (PFMG), this integer parameter indicates the number of relaxation sweeps to use before coarsening/restriction. Default: 1.

`AMRFLDPostRelax` – when using the `AMRFLDSolType` 4 (PFMG), this integer parameter indicates the number of relaxation sweeps to use after interpolation/prolongation. Default: 1.

`AMRFLDSolPrec` – when using either of the `AMRFLDSolType` values 1 (BiCGStab) or 3 (GMRES), this integer indicates whether to use our Enzo-specific multi-level preconditioner. Nonzero values indicate use of the preconditioner. Default: 1 (on).

`AMRFLDSol_precmaxit` – when using `AMRFLDSolPrec`, this indicates the maximum number of preconditioner iterations. Default: 1.

`AMRFLDSol_precJacit`† – when using `AMRFLDSolPrec`, this indicates the number of Jacobi relaxation iterations to use on the full Enzo AMR hierarchy. Default: 2.

`AMRFLDSol_precrelax`† – when using `AMRFLDSolPrec`, this integer parameter indicates the relaxation/smoother algorithm to use within the coarse grid PFMG solver. Allowed values include: 0 (Jacobi), 1 (weighted Jacobi), 2 (red-black Gauss-Seidel, symmetric), 3 (red-black Gauss-Seidel, nonsymmetric). Default: 1.

`AMRFLDSol_precnpre`† – when using `AMRFLDSolPrec`, this indicates the number of relaxation sweeps to use before coarsening/restriction within the coarse grid PFMG solver. Default: 1.

`AMRFLDSol_precnpost`† – when using `AMRFLDSolPrec`, this indicates the number of relaxation sweeps to use after interpolation/prolongation within the coarse grid PFMG solver. Default: 1.

`AMRFLDSol_precrestol`† – when using `AMRFLDSolPrec`, this floating-point parameter indicates the relative residual tolerance to use in stopping the preconditioner. Default: 0 (off, preconditioner stops based on iteration count).

`AMRFLDLimiterRmin`† – floating point value specifying the dimensionless constant in the definition of $R_{\rm min}$ in equation (67). This value must be non-negative. Default: 10^{-2}.

`AMRFLDLimiterDmax`† – floating point value specifying the dimensionless constant in the definition of $D_{\rm max}$ in equation (67). This value must be strictly positive. Default: 10^{-2}.

5.2 Extending AMR-FLD

(to be added...)

References

[1] J. Hayes and M. Norman, *Beyond flux-limited diffusion: Parallel algorithms for multidimensional radiation hydrodynamics*, The Astrophysical Journal, 147 (2003), pp. 197–220.

[2] J. E. Morel, *Diffusion-limit asymptotics of the transport equation, the $p_{1/3}$ euqations, and two flux-limited diffusion theories*, J. Quant. Spectrosc. Radiat. Transfer, 65 (2000), pp. 769–778.

[3] P. Paschos, *On the Ionization and Chemical Evolution of the Intergalactic Medium*, PhD thesis, University of Illinois at Urbana-Champaign, 2005.